



OPEN ACCESS

EDITED BY

Cinzia Tornatore,
National Research Council (CNR), Italy

REVIEWED BY

Jinlong Liu,
Zhejiang University, China
Aleksandar Ašonja,
Business Academy University (Novi Sad), Serbia

*CORRESPONDENCE

Octavio Armas,
✉ Octavio.Armas@uclm.es

RECEIVED 24 February 2025

ACCEPTED 01 April 2025

PUBLISHED 25 April 2025

CITATION

Corral-Gómez L, Armas O, Moya-Fernández F, A. Soriano J, Martos FJ and Nogueira J (2025) Effect of low-carbon paraffinic fuels on spray evolution under typical operating conditions for piston-engine aircrafts. *Front. Mech. Eng.* 11:1582708. doi: 10.3389/fmech.2025.1582708

COPYRIGHT

© 2025 Corral-Gómez, Armas, Moya-Fernández, A. Soriano, Martos and Nogueira. This is an open-access article distributed under the terms of the [Creative Commons Attribution License \(CC BY\)](https://creativecommons.org/licenses/by/4.0/). The use, distribution or reproduction in other forums is permitted, provided the original author(s) and the copyright owner(s) are credited and that the original publication in this journal is cited, in accordance with accepted academic practice. No use, distribution or reproduction is permitted which does not comply with these terms.

Effect of low-carbon paraffinic fuels on spray evolution under typical operating conditions for piston-engine aircrafts

Lis Corral-Gómez¹, Octavio Armas^{1*},
Francisco Moya-Fernández¹, José A. Soriano¹,
Francisco J. Martos² and José Nogueira¹

¹Universidad de Castilla-La Mancha, Campus de Excelencia Internacional en Energía y Medioambiente, Escuela de Ingeniería Industrial y Aeroespacial, Instituto de Investigación Aplicada a la Industria Aeronáutica, Toledo, Spain, ²Universidad de Málaga, Escuela de Ingenierías Industriales, Málaga, Spain

The evolution of the main macroscopic parameters that characterize spray formation for three different fuels is studied by means of the Schlieren visualization technique. The analyzed fuels comprise a fossil diesel fuel, used as reference, and two neat low carbon liquid 100% paraffinic fuels: a gas-to-liquid (GtL) and a hydrotreated vegetable oil (HVO). Additionally, the paper exposes the behavior of fuels autoignition for different injection pressures and start of energizing (SoE), for prescribed thermodynamic variables inside the engine cylinder. The experimental results obtained at the beginning of the injection process are compared with results from known models of penetration and cone angle of the fuel spray under non-evaporative conditions. These conditions are chosen to match those of the diesel engines used in surveillance light aircraft such as small helicopters. This work presents two important novelties: (i) the application of an automatic image analysis procedure (previously published) to the fuel injection process and (ii) the comparison of different fuels, regarding their effect on the injection process and the start of combustion. This is done under complete replacement of fossil fuel by two 100% paraffinic fuels. The most important results are the following: i) Compared to GtL and Diesel fuels, the HVO fuel has shorter ignition delay. This result could be attributed to its higher cetane number. ii) However, in most of the tested cases, in addition to a slightly longer spray penetration of the HVO fuel, its cone angle is also slightly wider than that of the other two fuels. This result would be collaborating in the development of a wider spray surface during the evolution of the spray lift off and beyond. This leads to a better air entrainment, and, in consequence, to produce an additional shortening of the ignition delay compared to the other two fuels. These findings would facilitate the fine tuning of modern engine technology for a progressive introduction of mentioned low carbon fuels in light aircraft such as unmanned helicopters for surveillance.

KEYWORDS

paraffinic fuels, piston engines, schlieren visualization, spray characterization, small aircraft

1 Introduction

Along the last years, small and medium size helicopters, used as surveillance unmanned aerial vehicles, have been powered by reciprocating internal combustion engines, i.e., aviation piston engines (Ning et al., 2020). In military applications, UAV engines have required not only high-power performance, but also high levels of stability and safety for tasks such as of intelligence, surveillance, and reconnaissance (ISR) missions (Schihl et al., 2015; Jing et al., 2015). Aviation piston engines have two modes of combustion: compression ignition (CI) and spark ignition (SI). These engines are undergoing a transition from gasoline to heavier fuels such as diesel due to its low volatility, high viscosity, and greater safety in storage and transportation; shifting from SI to CI (Chen et al., 2017; Ning et al., 2019).

Since the early 2000s diesel piston engines have been introduced in the aeronautical market. Their main advantage being the possibility to use aviation kerosene like Jet A1 instead of Avgas (aviation gasoline, like 100LL) and an smaller specific fuel consumption. This means double economical savings using less expensive fuel and at smaller quantities. Soon the flying schools accepted these engines to power their light aircrafts like the Cessna 172. Although helicopter stationary flight demands higher power than airplanes, these engines have evolved increasing their power to weight ratio and start to be an option for light helicopters. This interest triggered the study presented in this paper. Additionally, in the near future, the possibility of using diesel engines for small helicopters is going to meet further requirements. The European aeronautical regulations are forcing a shift from fossil fuel to SAF (Sustainable Aviation Fuels), carbon neutral. EASA (European Union Aviation Safety Agency) has imposed on European airlines to include a minimum content of 2% of SAF in their fuel for 2025, 6% in 2030 and 70% in 2050. This means that engines conceived for using aviation kerosene should also foresee the possibility of using SAFs like the HVO or Power to Liquid fuels. In this paper GtL is tested as an available precursor of Power to Liquid and HVO as a SAF by itself.

When diesel fuel is burned inside compression ignition engines, substances are generated that are harmful to the environment and to people's health (Dinc and Otkur, 2021; Arkoudeas et al., 2003; Gowdagiri et al., 2014). Nitrogen oxides (NO_x), carbon monoxide (CO) and particulate matter (PM) emissions are regulated by emissions legislation (EASA, 2019; Neves et al., 2020). Besides the improved efficiency of diesel engines, characterised by lower CO_2 emissions, it is desirable to reduce the rest of pollutant emissions. This remains an important research focus. For years biodiesel has been attractive alternative for reducing polluting emissions and as a substitute for diesel. But some of its disadvantages are the high cost of the raw material, the low calorific value, the high NO_x emissions, the formation of deposits, the problem of stability during storage, the poor cold properties and the rapid aging of the engine oil (Moser, 2009; Aatola et al., 2009). In addition, it had already been predicted that in the coming years biodiesel would have to face competition from Hydrotreated Vegetable Oil (HVO) and Gas to Liquid (GtL) (Ramos et al., 2016; Armas et al., 2015; Gómez et al., 2016).

HVO is a sustainable renewable fuel obtained through the hydrotreatment and isomerization of fatty organic waste. This

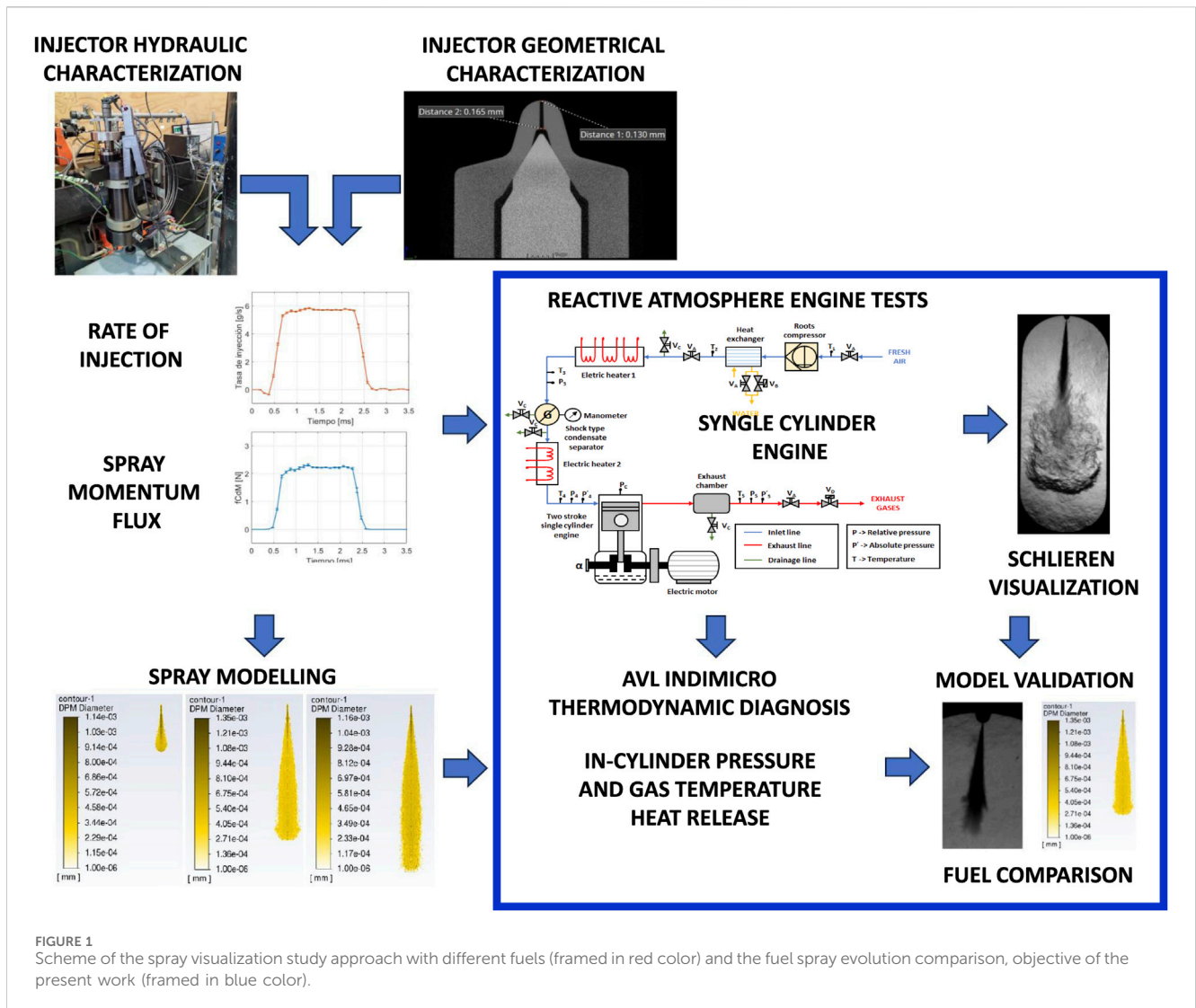
fuel is made up of a group of paraffinic hydrocarbons with no sulfur or aromatic content. This leads to a reduction of NO_x and PM emissions (Bohl et al., 2018; Sugiyama et al., 2012). HVO fuel has a higher cetane number (CN) and lower density compared to diesel (Erkkilä et al., 2011). A higher CN leads to a reduced ignition delay and, in consequence, to a smaller heat release during its shorter premixed combustion process (Alkhatat et al., 2021). On the other hand, the lower calorific value (LHV) of HVO fuel and diesel are very similar, so it is not necessary to make large changes on the amount of injected fuel to achieve an equivalent energy release (da Costa et al., 2022).

GtL is a fuel synthesized from natural gas through the Fisher-Tropsch process (Amhamed et al., 2024). This fuel is sulfur free, its amount of aromatic compounds is negligible and the proportion of carbon to hydrogen is lower, leading to a decrease in the formation of soot (Schaberg et al., 2005). Like HVO fuel, GtL fuel has less ignition delay than diesel due to a lower density and a higher CN. These particular properties mean that the generation of CO, NO_x and PM emissions is reduced (Wu et al., 2007).

To successfully employ sustainable paraffinic fuels in current and future thermal engines, it is essential to study the development of the fuel spray under conditions as close as possible to those of the combustion chamber where it will be injected. From a macroscopic perspective, the development of the spray cone angle and its penetration into the combustion chamber are parameters that define the air entrainment process during spray lift off. This affects the air-fuel mixing process and, consequently, the combustion process. Finally, the effectiveness of the combustion process simultaneously determines the engine's performance level and the regulated pollutant emissions generation. This reality is a fundamental factor for studying the fuel sprays and for contributing to determine the viability of using new fuels, (Gopinath et al., 2020).

The fuel spray characteristics of different fuels differ from each other because the physical properties of the fuels are different (Hulkkonen et al., 2011; Geng et al., 2021). Kook and Pickett (2012) studied spray macroscopic parameters such as spray penetration and cone angle for diesel and GtL fuels in a constant volume chamber. The experimental tests were carried out under similar operating conditions to those found in a compression ignition engine. As a result, the authors obtained a lower spray penetration for the GtL fuel compared to the diesel fuel. This could be due to the faster evaporation characteristics of the GtL fuel. Choi et al. (2015) also studied the spray macroscopic parameters of GtL and diesel fuels in a compression ignition engine and determined that the cone angle of GtL fuel was larger than that of diesel fuel. Bohl et al. (2017) determined the macroscopic parameters of the HVO fuel spray and compared it with diesel fuel. During experimental tests, the authors heated the fuels to 80°C to achieve an environment similar to that of a compression ignition engine. They determined that HVO fuel has lower spray penetration and a higher spray cone angle compared to diesel fuel, resulting in a more distributed air-fuel mixture.

The objective of this work is to contribute to determining the spray macroscopic parameters and the ignition delay of HVO, GtL and diesel fuels. It is also important to evaluate the spray surface interface with the surrounding air inside the combustion chamber. To achieve this, an experimental facility based on a CI engine with optical accesses is used. It allows visualizing the injection and



combustion process. The Schlieren optical technique is used to acquire images of the fuel injection event and its subsequent combustion. The experimental tests are carried out at different injection pressures and different injector starts of energization (SoE), to determine their influence (i) on the macroscopic parameters, (ii) on the ignition delay and (iii) on the spray surface.

2 Materials and methods

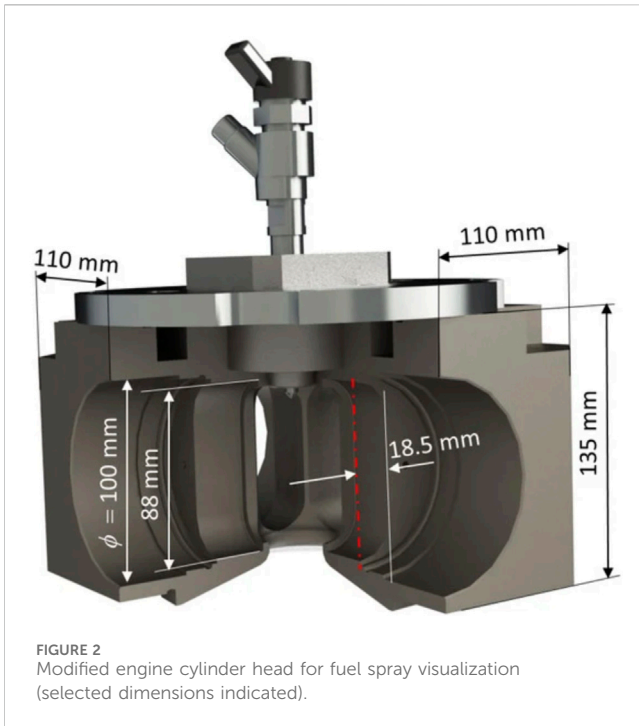
2.1 Experimental facility

This work is part of a larger research project. Figure 1 presents the complete methodological statement of the whole project, highlighting the particular objective of the part published in this manuscript. The relevant parts of experimental installation used in this manuscript are described along the following text.

In an actual CI engine, the length of the diesel spray is determined by either (i) the diameter of the pre-combustion chamber (in an indirect injection combustion engine) or (ii) the piston bowl (in the case of direct injection combustion engines).

This length, for an automotive engine, can measure between 18 and 50 mm before hitting the wall. However, in most cases, the spray hits the bowl wall before the atomization process is complete. This is the reason why it is important to study the jet lengths up to 100 mm, a length long enough for the jet to complete its atomization.

The engine used in this work is an adapted version of a Jenbacher JW-50 two-stroke, single-cylinder diesel engine with 3 L displacement, with cylinder diameter of 150 mm; geometrical stroke of 170 mm; effective stroke of 108 mm, total original geometric compression ratio of 26.3/1, original effective compression ratio of 17.1/1, and maximum rotational speed of 700 min⁻¹. The engine was modified for visualization purpose of injection and combustion processes. After the engine cylinder head modification, the effective compression ratio is around 9.5/1. The modified engine torque and power depend on the boost pressure and quantity of fuel injected. The limitation to their value is a maximum pressure of 10 MPa, along the cycle, to avoid the breakage of the quartz windows. More details about the modified engine can be found at Corral-Gómez et al. (2022). Figure 2 shows the modified cylinder head. It has four accesses at the four sides, and a fifth one at the top. The in-cylinder pressure sensor is mounted in one of the

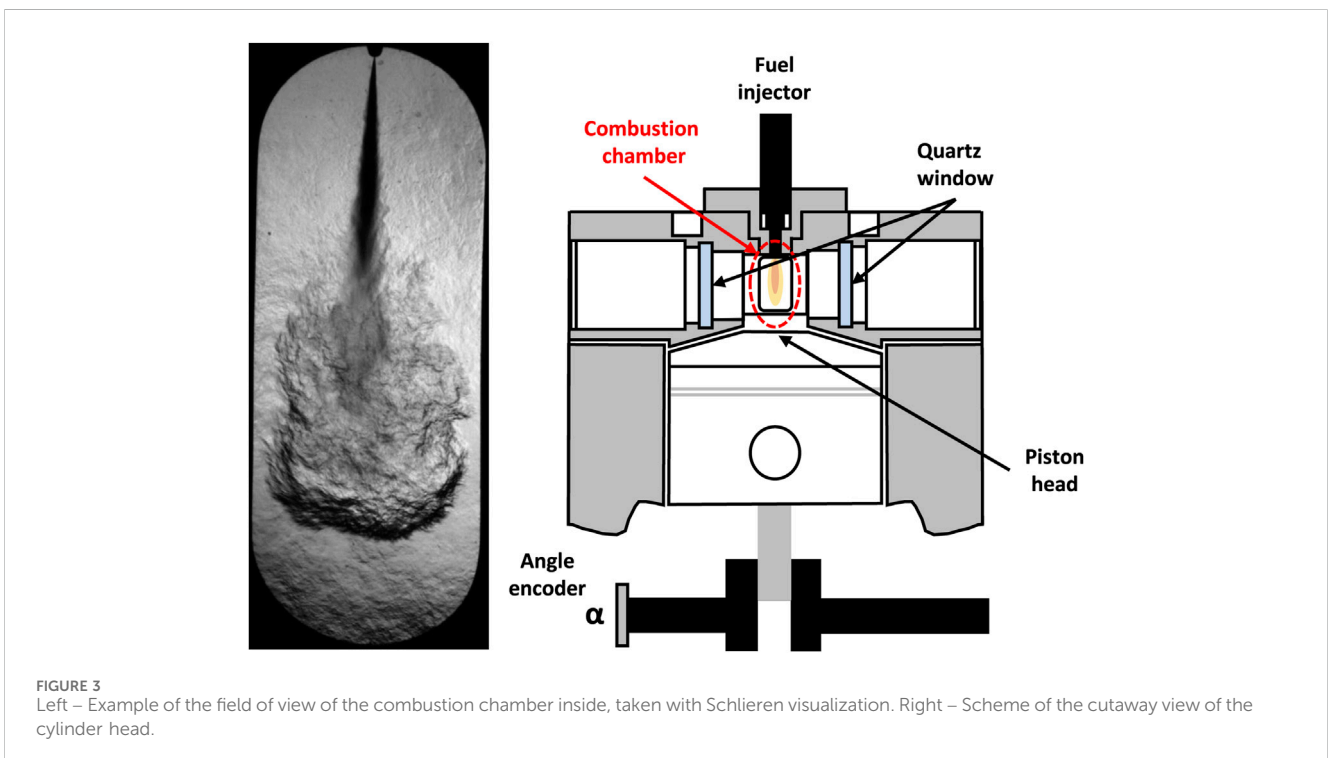


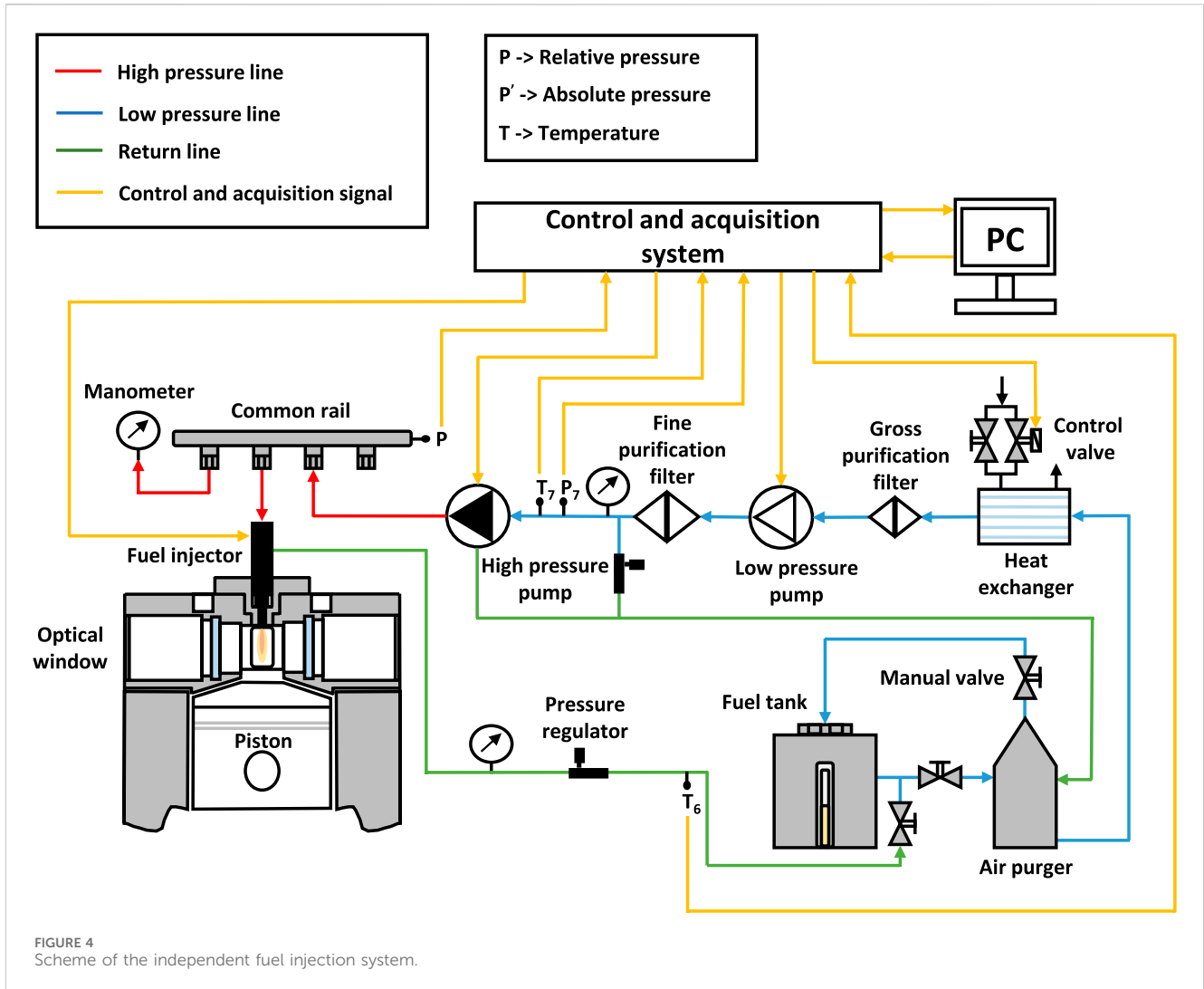
lateral accesses, while quartz windows (L88 × W37 × E28, with corner radii of R18 mm) are installed in the other three accesses. The quartz windows support a maximum pressure of 10 MPa and a maximum temperature of 1350 K. The upper access (D24 × L10.5 mm), on top of the cylinder head, is used to allocate the fuel injector (Corral-Gómez et al., 2023b). Figure 3 shows at cutaway view of the cylinder head and an example of the

field of view of the combustion chamber inside, taken with Schlieren visualization.

The operating conditions have been chosen to be representative of the ones related to aeronautical diesel engine. A usual matching is made by assuring just the same air density, as this matches many processes (e.g., Equation 1). But, in this study, the parameters involving spray formation and evolution force the matching of the whole thermodynamical state (i.e., Temperature and Pressure). The conditions selected span from one extreme case (a) corresponding to 2.82 MPa and 778 K for SOE at 4° before TDC; down to the other limit case (b) of 1.88 MPa and 693 K for SOE at 18° before TDC. Regarding these conditions, a basic comparison can be made with those meet in a typical aeronautical Diesel engine like CD-135 (based on the Mercedes-Benz OM640), that powers aircrafts up to a service ceiling of 24,000 feet (7,315 m). This engine is characterized by SOE around 15.7° before TDC, geometrical compression ratio of 18:1 and supercharger pressure ratio of 2:1. Measurements of the indicated cycle (Mihyar et al., 2023) indicate that the effective compression ratio from the environment to the SOE event is: 47.8. Thus, the commented case (a) corresponds to the operation of this engine at an altitude of 13,900 ft (4,236 m) and ISA -6 (6° below the International Standard Atmosphere). This is a common condition for flying over USA or Middle Europe. While the commented case (b) corresponds to an altitude of 23,700 ft (7,223 m) and ISA - 33. An extreme condition, usual if flying over Canada or North Europe in winter. Cold cases have been selected as they compromise engine functioning to a higher degree than hot ones.

During the experimental tests the engine speed (n) is kept constant at 500 min^{-1} , driven by an asynchronous electric motor. The temperature of the cylinder head and the engine is conditioned





with a separated and externally controlled lubrication-cooling system. This system sets the temperature of cooling water and lubricating oil of the engine at 333 K. Five resistors placed in the inlet line are used to set the intake air temperature (T_a) to 323 K and a root compressor increases the intake air pressure (P_a) to 0.13 MPa. An injection is made every 64 cycles to keep the thermodynamic conditions of the in-cylinder constant and to reduce the mechanical and thermal stresses of the quartz windows. A solenoid fuel injector with a single-hole axial nozzle has been used. The nozzle has a hole diameter of 0.115 mm and a K-factor of 3.5 has been used. The parameters of fuel temperature, Start of energization (SoE), injection pressure and injector energization time are controlled and monitored from the control system of the experimental facility. Figure 4 shows the scheme of the injection system. The system is equipped with a Bosch common-rail system with a capacity of 20 cm³ that allows it to reach injection pressures up to 130 MPa, (Corral-Gómez et al., 2023b).

Thermodynamic diagnosis was carried out using an AVL IndiMicro 602 (which includes an in-cylinder pressure sensor GH14P and its glow plug adaptor) and an AVL IndiCOM 2013 (2.5) system for combustion analysis. Crankshaft rotational speed and instantaneous piston position were determined by means of an

angle encoder (Kistler 2614CK) with a resolution of 720 pulses per revolution (0.5 crank angle degree), (Martos et al., 2023).

2.2 Visualization system and image processing

The visualization system used in the experimental facility is the Schlieren optical technique. This technique allows the detection of the variation of the density gradients of an in-homogeneous and transparent medium (Settles, 2001). The Schlieren system setup, presented in Figure 5, is divided into two sections: lighting and collection. The lighting section comprises a 150 W lamp, a focusing lens of $f = 50.3$ mm and a parabolic mirror of $f = 1,000$ mm. The light source (lamp and focusing lens) is located at the focal point of the parabolic mirror, forming an array or parallel light beams. The collection section comprises another parabolic mirror of $f = 1,000$ mm and a Fastcam nova S6 high-speed camera. The parabolic mirror collects the light and focuses it on the high-speed camera.

The control software allows to synchronize the acquisition of the images of the fuel spray and the injection event. To do this, based on

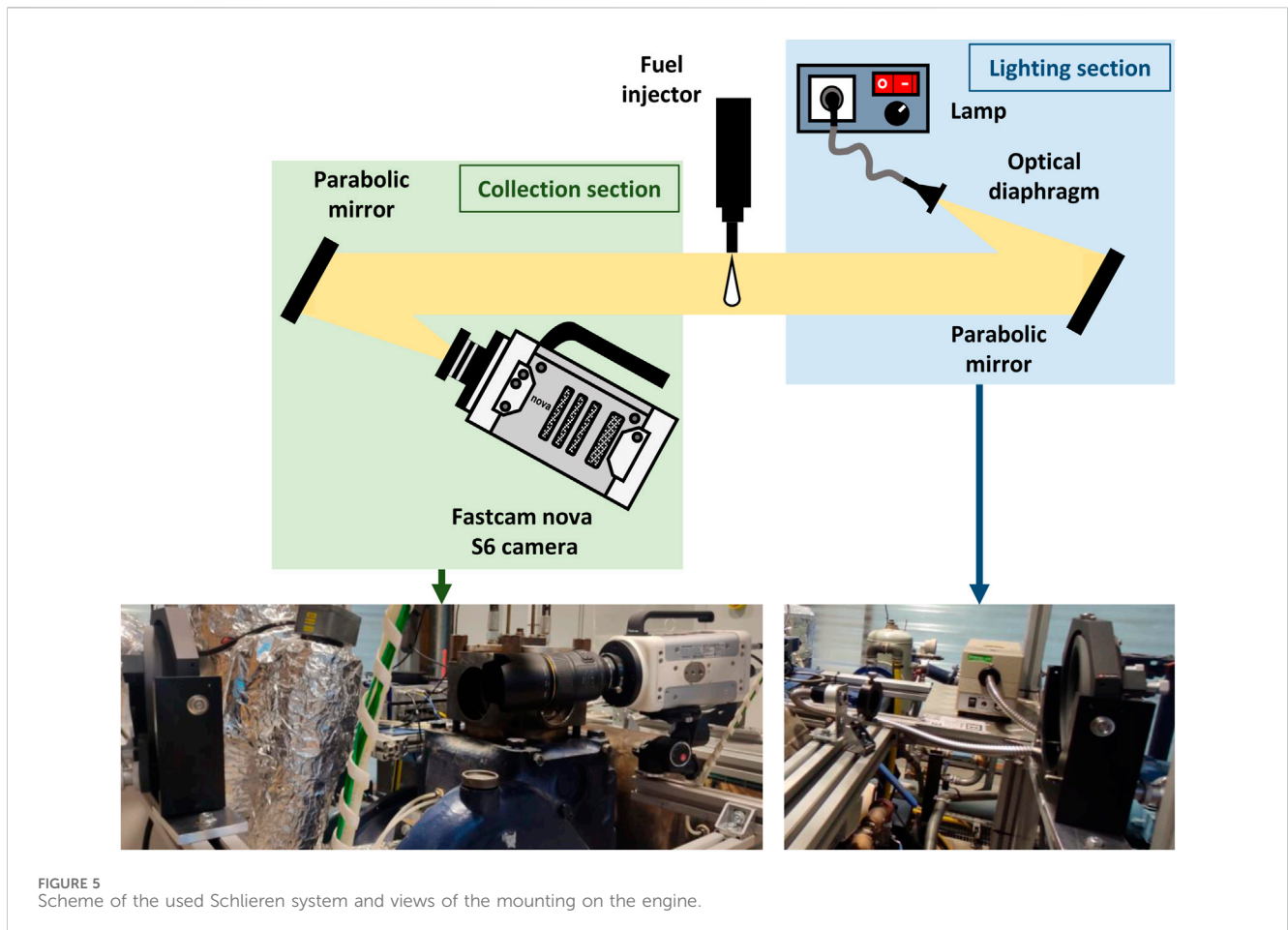


FIGURE 5 Scheme of the used Schlieren system and views of the mounting on the engine.

TABLE 1 Configuration of the parameters of the high-speed camera used for the experimental tests.

Properties	Value	Units
Frame rate	15,000	FPS
Sample time	60.67	μs
Shutter speed	40	μs
Image resolution	896×512	pixels
Resolution	10.5	pixel/mm

the crankshaft angle, the software sends a trigger signal to the high-speed camera and the fuel injector. In each experimental test, 100 images are taken, of which 10 of them are taken before the injection and 90 of them afterwards. 5 repetitions were made for each experimental test to reduce the uncertainty due to the natural engine cyclic dispersion. The images taken have a depth of 12 bits, so 0 is represented as black color and 4,095 as white color. Table 1 shows the configuration of the parameters of the high-speed camera used for the experimental tests.

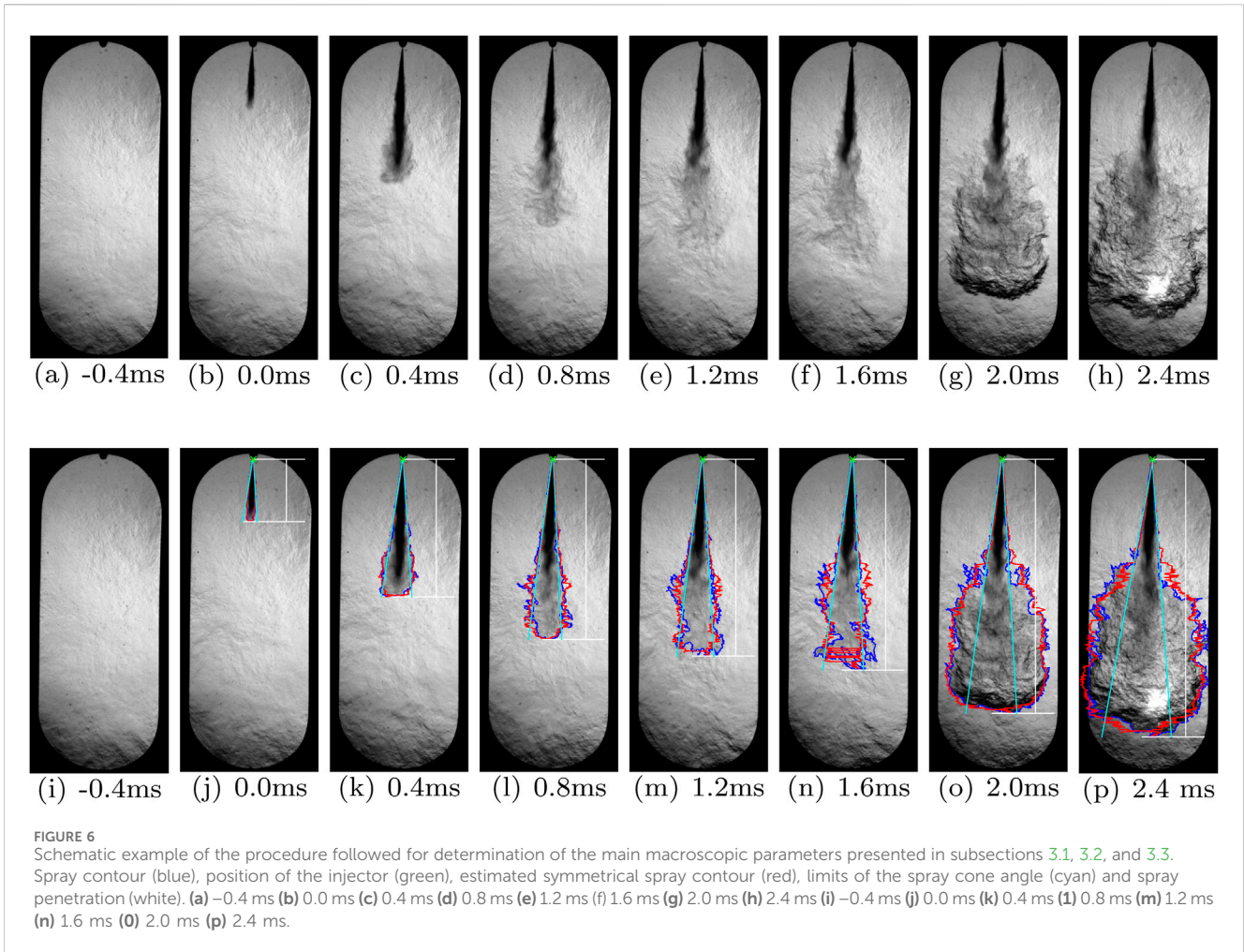
The image processing technique used, is suitable for studying the macroscopic parameters of the fuel spray (Soid and Zainal, 2011). It has been applied with the help of an algorithm developed in Matlab[®] software, described in more detail in Corral-Gómez et al. (2023b). It

allows to obtain the contour of the fuel spray by processing the images obtained during the experimental tests. This contour provides the fuel spray, the spray penetration, cone angle and area, following Ma et al. (2016), Rubio-Gómez et al. (2018), Corral-Gómez et al. (2019). With these parameters, and the thermodynamic conditions in the chamber, it is possible to estimate the fuel spray interface with the surrounding air, the fuel spray volume and the ignition and injection delays.

Figure 6 shows a schematic example of the procedure followed for determination of the main macroscopic parameters such as: spray penetration, cone angle and estimated spray surface using the automatic procedure previously published in Corral-Gómez et al. (2023b) and commented in Section 3 of the present work. In addition, the mentioned procedure also helps to automatically determine the start of injection and the ignition delay from the image analysis. The present work constitutes a direct application of the above cited methodology.

2.3 Spray penetration and cone angle models

The spray atomisation process depends on variables of the conditions in the combustion chamber, the injection conditions (Corral-Gómez et al., 2023c) and the fuel (Martos et al., 2022). The thermophysical properties of the fuel, such as density and viscosity,



significantly affect the flow of the fluid in the injector and consequently the formation of the spray (Martos et al., 2022).

As it is commented in the results section, the first instants of the experimental evolution of the penetration and cone angle of the sprays for the different studied fuels are compared with the evolution predicted by known models proposed under non-evaporative conditions. The models used for the aforementioned comparison are described below.

Desantes et al. (2006) proposed a model to determine the transient spray penetration in a non-evaporative and quiescent environment as a function of the momentum flux, \dot{M}_f , the ambient density, ρ_a , the spray cone angle, θ and of course the time, t , Equation 1.

$$S(t) = K_1 \dot{M}_f^{0.25} \rho_a^{-0.25} t^{0.5} \tan^{-0.5} \left(\frac{\theta}{2} \right) \quad (1)$$

From an experimental fitting, Desantes et al. (2006) proposed a value of the proportionality constant K_1 of 1.26. The momentum flux is the fuel mass flow rate, \dot{m}_f , multiplied by the fuel velocity at the nozzle exit, u , i.e., $\dot{M}_f = \dot{m}_f u$. The fuel mass flow rate depends on the theoretical fuel velocity at the nozzle exit obtained from the Bernoulli equation, u_B , the fuel density, ρ_f , and the hole area, A_h , via a discharge coefficient, c_d , Equation 2.

$$\dot{m}_f = C_d \rho_f A_h u_B = \frac{\pi}{4} C_d D_h^2 \sqrt{2 \rho_f (P_{inj} - P_a)} \quad (2)$$

In Corral-Gómez et al. (2023c) a correlation of the discharge coefficient as a function of injection pressure, P_{inj} , and nozzle hole diameter, D_h , was obtained for three different nozzles, including the one tested in this research work. The Equation 3 shows this correlation applied to the nozzle with a hole diameter of 0.115 mm, for P_{inj} expressed in MPa.

$$C_d = 0.8332 + 3.759 \cdot 10^{-6} P_{inj} \quad (3)$$

Considering phenomena such as cavitation or velocity profile, the fuel velocity at the nozzle exit can be a function of the theoretical velocity, u_B , by means of a velocity coefficient, C_v , i.e., $u = C_v u_B$, (Payri et al., 2020). Taking Equation 2 into account, the momentum flux can be determined with Equation 4.

$$\dot{M}_f = C_d \rho_f A_h u_B u = \frac{\pi}{2} C_d C_v D_h^2 (P_{inj} - P_a) \quad (4)$$

Substituting Equations 3, 4 into Equation 1 and grouping all constants and coefficients into K , so that $K = 1.26 (C_v \cdot \pi/2)^{0.25}$, gives Equation 5 with which the spray penetration can be determined. The velocity coefficient, although unknown, is of the order of and slightly higher than the discharge coefficient since the

relationship between them is the so-called area coefficient, which is close to unity.

$$S(t) = K C_d^{0.25} D_h^{0.5} (P_{inj} - P_a(t))^{0.25} \rho_a(t)^{-0.25} t^{0.5} \tan^{-0.5}\left(\frac{\theta}{2}\right) \quad (5)$$

In Equation 5, the discharge coefficient defined in Equation 3 is used. Additionally, both the pressure and the density of the gas inside the combustion chamber have been considered to be transient, using their variation to calculate the corresponding increments of $S(t)$ in a time marching algorithm.

Siebers (2009) proposed a model to determine the spray cone angle, θ , as a function of the density of the gas inside the combustion chamber and the density of the injected fuel, ρ_f , Equation 6.

$$\tan\left(\frac{\theta}{2}\right) = c_1 \left[\left(\frac{\rho_a}{\rho_f}\right)^{0.19} - c_2 \left(\frac{\rho_f}{\rho_a}\right)^{0.5} \right] \quad (6)$$

In Equation 6 the constant c_1 depends only on the geometry of the nozzle. This coefficient can take values in the range [0.26 – 0.40]. The constant c_2 is zero for non-evaporating sprays and 0.0043 for vaporising sprays, (Naber and Siebers, 1996; Hiroyasu, 1980), as is the case here.

The constant c_1 is unknown. As it depends only on the nozzle geometry, this constant is the same regardless of the fuel used. It has been obtained by fitting the spray cone angle obtained experimentally for all tested modes with Equation 6. A value of c_1 equal to 0.3007 has been obtained, this fit had a mean square error of 0.5721.

The validation of the models used in this work, usually employed with fossil diesel fuel, are described in detail in Desantes et al. (2006). However, to be able to use these models with HVO and GtL fuels, parameters such as fuel bulk modulus, fuel injection rate, and/or spray momentum flux have been experimentally validated in previous works (Armas et al., 2016; Payri et al., 2020; Corral-Gómez et al., 2023a) respectively. Also, they have been previously applied to modeling works such as Martos et al. (2022), Corral-Gómez et al. (2023c).

2.4 Fuels

As commented in the introduction, in this study, three fuels have been considered to carry out the experimental tests. The fuels are a HVO fuel supplied by Repsol (Spain), a GtL fuel supplied by SASOL (South Africa) and obtained through a Fischer-Tropsch process, and a conventional fossil diesel fuel without any biodiesel addition, supplied by Repsol (Spain). The last one is used as reference fuel in this work. The main physicochemical properties of fuels are detailed in Table 2. The tested fuels can be used in Diesel engines with application in propulsive systems for land transport, Soriano et al. (2019).

2.5 Test matrix

Table 3 shows the general experimental conditions for the engine used along the test matrix, to obtain the spray

TABLE 2 Main properties of the tested fuels.

Properties	Diesel	HVO	GtL
C (% w/w)	86.2	85.7	84.7
H (% w/w)	13.8	14.3	15.3
Density at 15°C (kg/m ³)	835.8	779.1	773.1
Density at 40°C (kg/m ³)*	827.6	763.5	756.9
Viscosity at 40°C (cSt)	2.96	2.87	2.3
Cold Filter Plugging Point (K)	254	233	228
Flash point (K)	334	343	336
Cetane number	54.5	75.5	71
High Heating Value (MJ/kg)	45.97	47.24	46.91
Lower Heating Value (MJ/kg)	43.18	44.20	43.66
Distillation (vol.)			
10% (K)	479.5	538.2	468
50% (K)	548.9	551.5	533
90% (K)	617.9	563.4	611

*Calculated with Equations 9–11 of the work done by Armas et al. (2016).

TABLE 3 Test conditions of the experimental facility.

Parameters	Value	Units	Accuracy
Engine speed	500	min ⁻¹	±1
Injection pressure	50, 70, 90, 110	MPa	±0.05
Energization time	2	ms	±0.01
Fuel temperature	313	K	±0.1
Intake pressure	0.13	MPa	±0.05
Intake temperature	323	K	±0.1

TABLE 4 Accuracy and uncertainty of measured parameters during the fuel injection tests.

Parameters	Units	Operating range	Accuracy
Injection pressure	MPa	20 ... 130	±0.1
Back pressure	MPa	1 ... 18	±0.1
Energizing time	μs	80 ... 9999	±0.05
Number of injections	–		
Generator frequency	MHz	0.01 ... 10	±0.05
Current probe	A	±140	±1% ^a
Temperatures	°C	±70	±0.05
Weighted fuel mass	g	0 ... 4000	±0.025

^aIn ±100 mA.

macroscopic parameters, the estimation the spray surface and volume, and the ignition delay (ID) and the injector opening delay (IOD). Table 4 shows the experimental conditions for the

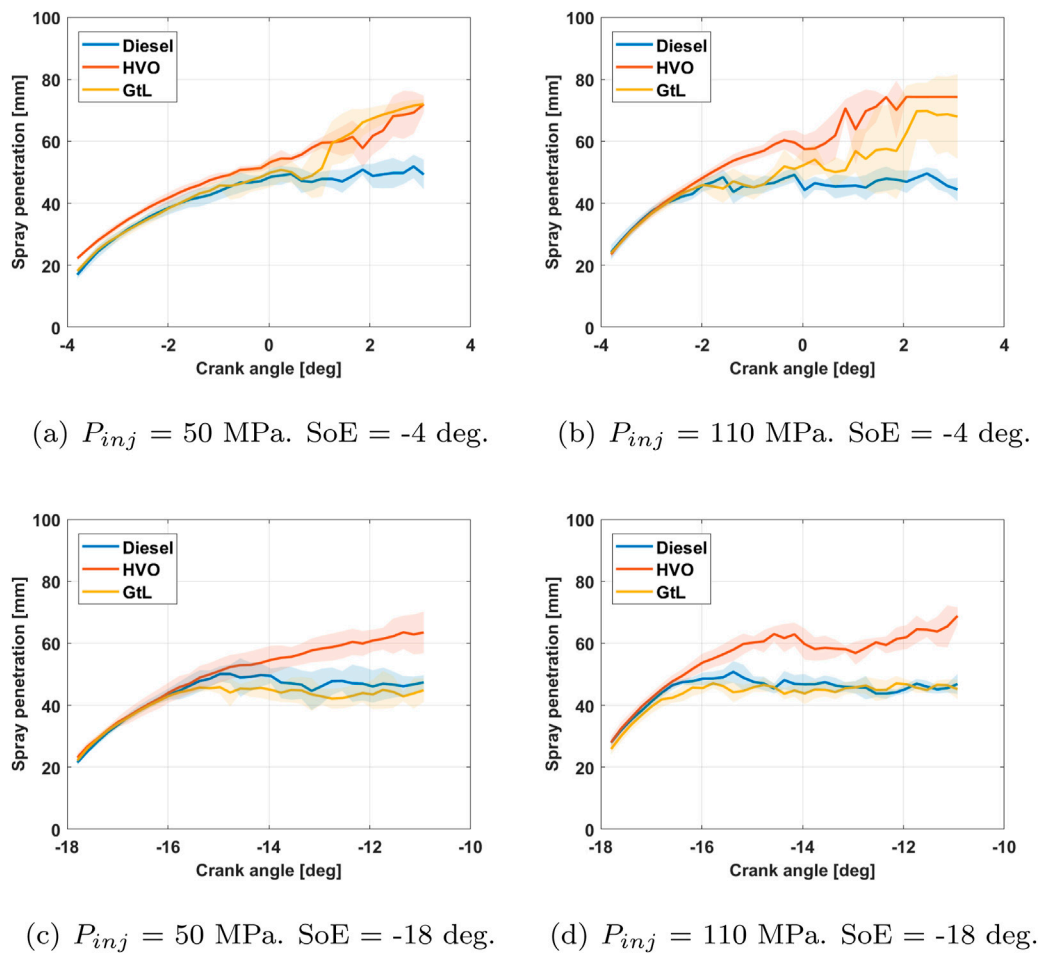


FIGURE 7 Spray penetration as a function of crank angle for each fuel. $n = 500 \text{ min}^{-1}$, $T_a = 323 \text{ K}$, $P_a = 0.13 \text{ MPa}$. (a) $P_{inj} = 50 \text{ MPa}$, SoE = -4 deg, (b) $P_{inj} = 110 \text{ MPa}$, SoE = -4 deg, (c) $P_{inj} = 50 \text{ MPa}$, SoE = -18 deg, (d) $P_{inj} = 110 \text{ MPa}$, SoE = -18 deg.

fuel injection system. The three fuels were operated under four injection pressures, one injection duration and one temperature. The intake air temperature and pressure during all the experimental tests were kept constant. The start of energization (SoE) is set to -4 , -6 , -8 , -10 , -12 , -14 , -16 and -18° from top dead center (TDC).

The injector used for the experimental tests is a Bosch solenoid injector with serial number 89909/0445110239, with a single-hole axial nozzle of 0.115 mm and a K-factor of 3.5. All the parameters of the experimental conditions are modified through the control system of the experimental facility.

3 Results and discussion

This section is divided into four subsections. [Subsection 3.1](#) exhibits the results of the spray macroscopic parameters: spray penetration and cone angle of fuels. Subsequently, [subsection 3.2](#) shows the results of the estimation of the spray surface determined for each of the experimental tests. [Subsection 3.3](#) exposes the results for the ignition delay. As commented before, for all fuels, the results shown were calculated as the average all fuels and for the five

injection events of each experimental test. The standard deviation of the individual measurements is also displayed for each calculated value and is shaded in the same color. After these results have been exposed, [subsection 3.4](#) indicates the coherence between existing models and the experiments.

3.1 Experimental spray macroscopic parameters: spray penetration and cone angle

[Figure 7](#) shows the spray penetration as a function of crank angle for each fuel. The results shown correspond to injection pressures of 50 and 110 MPa and to a start of energization (SoE) of -4 and -18° .

[Figure 7](#) shows that increasing the injection pressure produces a greater impulse of the fuel spray and results in a reduction of the stabilization time for the spray penetration. This behavior is similar to that reported in the literature by [Han et al. \(2017\)](#), [Algayyim and Wandel \(2021\)](#) and [ul Haq et al. \(2023\)](#). On the other hand, an earlier start of energization (SoE) results in the GtL fuel penetration being sharply reduced and behaving the same as diesel fuel. This is due to the low density and surface tension of the GtL fuel and the

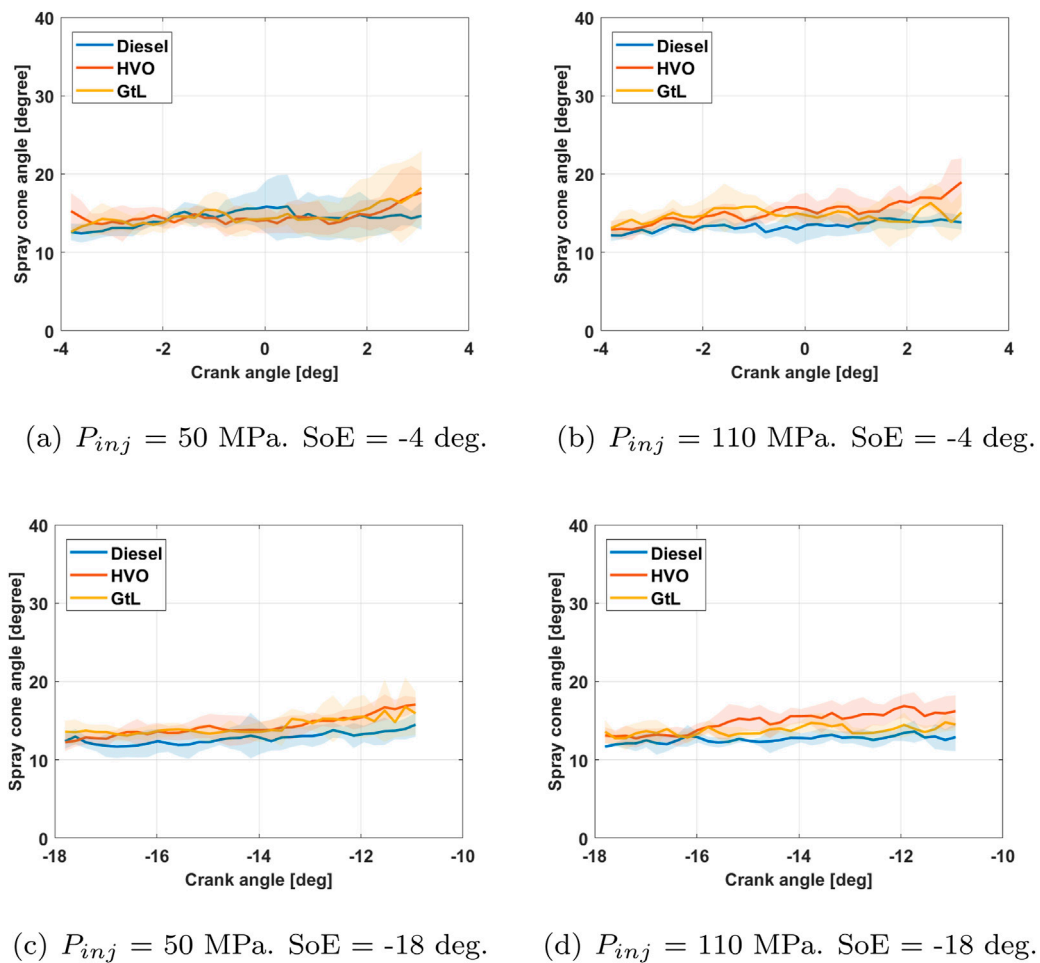


FIGURE 8

Spray cone angle as a function of crank angle for each fuel. $n = 500 \text{ min}^{-1}$. $T_a = 323 \text{ K}$. $P_a = 0.13 \text{ MPa}$. (a) $P_{inj} = 50 \text{ MPa}$, SoE = -4 deg, (b) $P_{inj} = 110 \text{ MPa}$, SoE = -4 deg, (c) $P_{inj} = 50 \text{ MPa}$, SoE = -8 deg, (d) $P_{inj} = 110 \text{ MPa}$, SoE = -18 deg.

reduction in the ambient density inside the cylinder as the start of energization (SoE) advances. A greater ambient density, a lower density and surface tension of the fuel favors better atomization of the fuel, and therefore greater penetration of the vapor phase of the spray. Besides, the distillation curve of GtL fuel is lower than that of diesel fuel and HVO fuel, so its evaporation is greater than that of these two fuels at the same temperature. This conclusion is consistent with the study carried out by Mancaruso et al. (2011). Finally, the penetration of diesel fuel and HVO fuel is hardly influenced by the modification of the start of energization (SoE).

Figure 8 shows the spray cone angle as a function of crank angle for each fuel. The results shown correspond to the injection pressures of 50 and 110 MPa and to a start of energization (SoE) of -4 and -18° .

Figure 8 shows that the spray cone angle is not influenced by the injection pressure, nor by the start of energization (SoE), nor by the properties of the fuel. In all experimental tests, a constant and very similar spray cone angle is obtained between the three fuels. This is because the spray cone angle is influenced by the injector geometry

and not by the injection parameters and fuel properties as determined in the work done by Fajri et al. (2023).

The differences in fuel properties obtained, while suggesting that the engine setup can be improved by fine-tuning, would not imply changing its original technology as has occurred in other studies but with other objectives, (Milojević et al., 2024).

The database obtained constitutes a novel contribution to the development, introduction and fine-tuning of new paraffinic fuels in the current propulsion systems used in different means of land, sea and even air transport. Indeed, experimental studies such as the one presented here generate a large amount of data. To make the most of this information, future work will employ statistical analysis techniques such as TOPSIS or Taguchi. These have already been used in the optimization of tribology studies of thermal engines, (Gajević et al., 2024).

Likewise, the management of the experimental information obtained in this work would allow the development of prediction models using techniques such as artificial intelligence or machine learning, (Marinković et al., 2024).

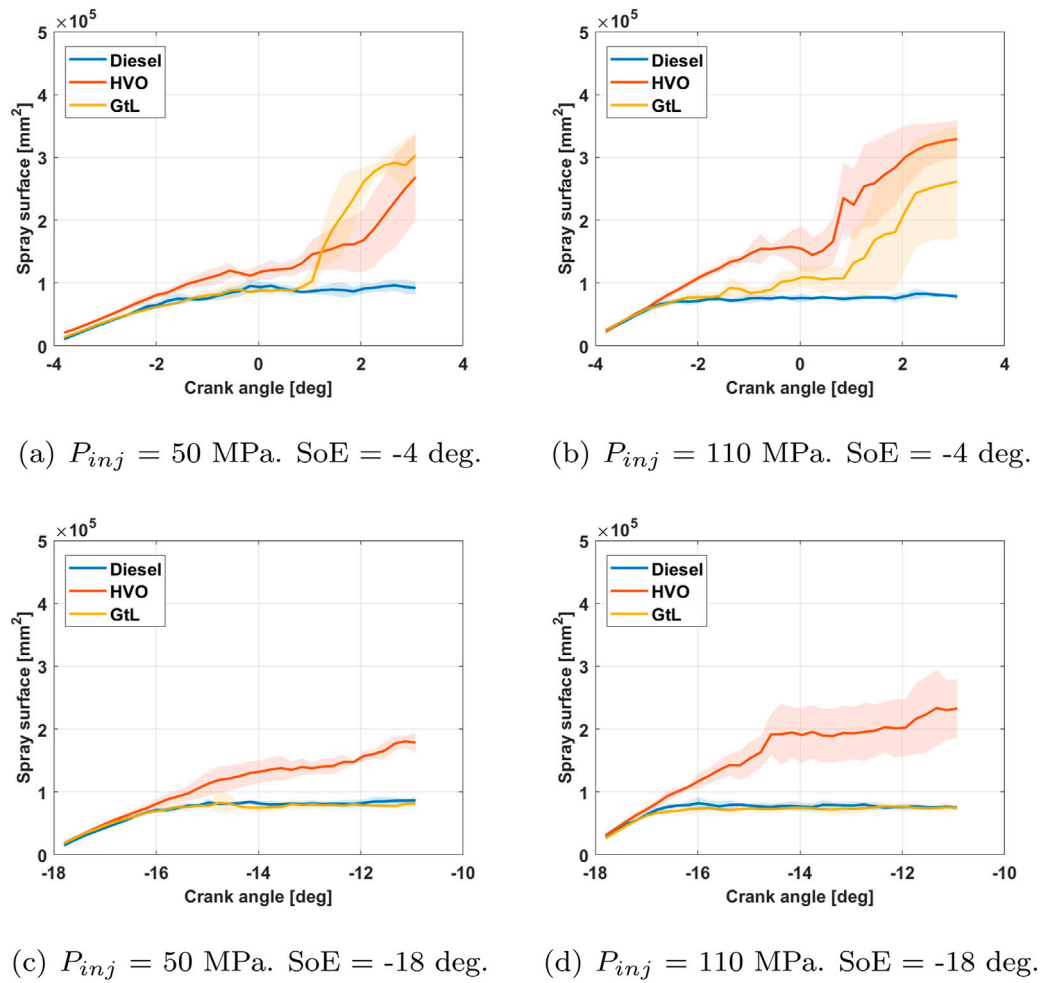


FIGURE 9 Estimation of the spray surface as a function of crank angle for each fuel. $n = 500 \text{ min}^{-1}$. $T_a = 323 \text{ K}$. $P_a = 0.13 \text{ MPa}$. (a) $P_{inj} = 50 \text{ MPa}$, SoE = -4 deg, (b) $P_{inj} = 110 \text{ MPa}$, SoE = -4 deg, (c) $P_{inj} = 50 \text{ MPa}$, SoE = -18 deg, (d) $P_{inj} = 110 \text{ MPa}$, SoE = -18 deg.

3.2 Estimation of spray surface

Air-fuel mixture performance is usually evaluated with the macroscopic parameters of the spray: the spray penetration and the cone angle of the fuel (Agarwal et al., 2013). With these two parameters the area of the spray is obtained. If a 180° rotation vertical of the spray area is made around the injection axis, the estimate of the spray volume is obtained. This volume has an external surface that is in direct contact with the air in the combustion chamber (Corral-Gómez et al., 2023b). Therefore, the larger the spray surface, the greater the contact with the air, and therefore, the greater the air-fuel mixture, the better the combustion will be and the fewer emissions will be emitted (Hansen et al., 2005). Figure 9 shows the estimation of the spray surface as a function of crank angle for each fuel. The results shown correspond to the injection pressures of 50 and 110 MPa and to a start of energization (SoE) of -4 and -18° .

Figure 9 shows that the spray surface has the same behavior as the spray penetration because the spray angle remains constant for the same injector geometry.

3.3 Estimation of ignition delay

The ignition delay is an important parameter which characterizes the initiation of the combustion process and consequently its development in Diesel engines. This parameter depends on fuel chemical characteristics, related to the fuel structure and its properties (chemical delay). It also depends on the thermodynamic engine operating conditions, related to physical processes such as fuel evaporation and mixing with surrounding air (physical delay). Although the main objective of this work is not the determination of ignition delay of the analyzed fuels, an estimation of this parameter is done. To know and control the fuel ignition delay is important for maximizing the indicated engine work (with penalizing combustion noise) and for minimizing the nitrogen oxides without penalizing the particulate matter emissions (Miron et al., 2021).

Figure 10 shows the start of injection (SoI) and the start of combustion (SoC) as a function of the start of the energization (SoE) comparing the three fuels for each injection pressure.

Figure 10 shows that the start of injection (SoI) does not vary in any of the experimental tests carried out, so neither the injection

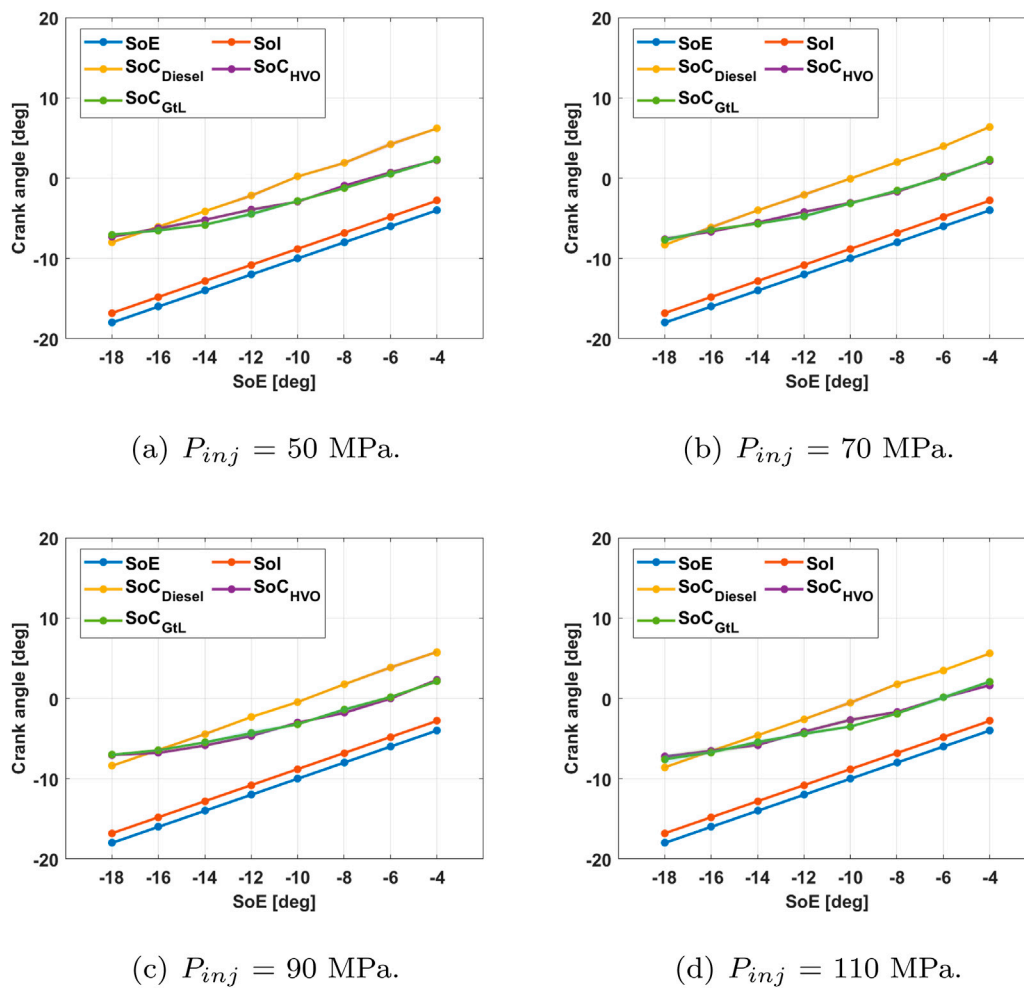


FIGURE 10

Start of energization (SoE), start of injection (SoI) and start of combustion (SoC) as a function of the start of the energization (SoE) comparing the three fuels for each injection pressures. $n = 500 \text{ min}^{-1}$, $T_a = 323 \text{ K}$, $P_a = 0.13 \text{ MPa}$. (a) $P_{inj} = 50 \text{ MPa}$, (b) $P_{inj} = 70 \text{ MPa}$, (c) $P_{inj} = 90 \text{ MPa}$, (d) $P_{inj} = 110 \text{ MPa}$.

pressure nor the start of energization (SoE) influence the injector opening delay (IOD). Regarding the start of combustion (SoC) both paraffinic fuels show differences with the fossil fuel. According to the results presented in Figure 10, for very advanced injection starts (-18°) and any of the injection pressures tested, the time between the start of injection (SoI) and the start of combustion (SoC) (assumed as “ignition delay”) was the same regardless of the fuel used. However, as the injection approaches the minimum of the in-cylinder volume (top dead center), the higher cetane number of the paraffinic fuels caused a significant reduction in the time between SoI and SoC when compared to diesel fuel, and similar for both of them. As can be seen, the automatic procedure is able to detect the different evolution of the “ignition delay” between Diesel fuel (with CN = 51) and both renewable fuels (with CN 75.5 and 71 for HVO and GtL respectively). In this case, the average relative difference between CN of Diesel fuel versus renewable fuels is around 44%. On the other hand, the relative difference in CN between both renewable paraffinic both fuels is only around 6%.

Figure 10 also shows, that the injection pressure was modified from 50 to 110 MPa (with a relative difference around 54%). With this magnitude of injection pressure variation, for all the injection

advances and fuels tested, it was expected that the ignition delay would decrease as the injection pressure increases and the injection advance is reduced with respect to the TDC (Chen et al., 2024). However, the results in Figure 10 do not show this trend. This behaviour would be explained as follows: i) in the range of injection pressure tested, with this type of engine, the effect of cetane number of fuels on ignition delay, seems to be more important than the effect of the injection pressure itself, and ii) the automatic procedure does not have sensibility enough to clearly detect variations in ignition delay in the range corresponding to the injection pressure variation tested. In any case, similar behaviour was reported by Bjørgen et al. (2020) and Aradi and Ryan (1995).

3.4 Spray penetration and cone angle. modelled and experimental comparison

For each fuel, Figure 11 shows the results obtained with the Equation 5 (dashed line) compared to the experimental results (solid line), for the tested extreme cases of injection pressure and SoE. Note that the model shown in Equation 5 of Desantes et al. (2006)

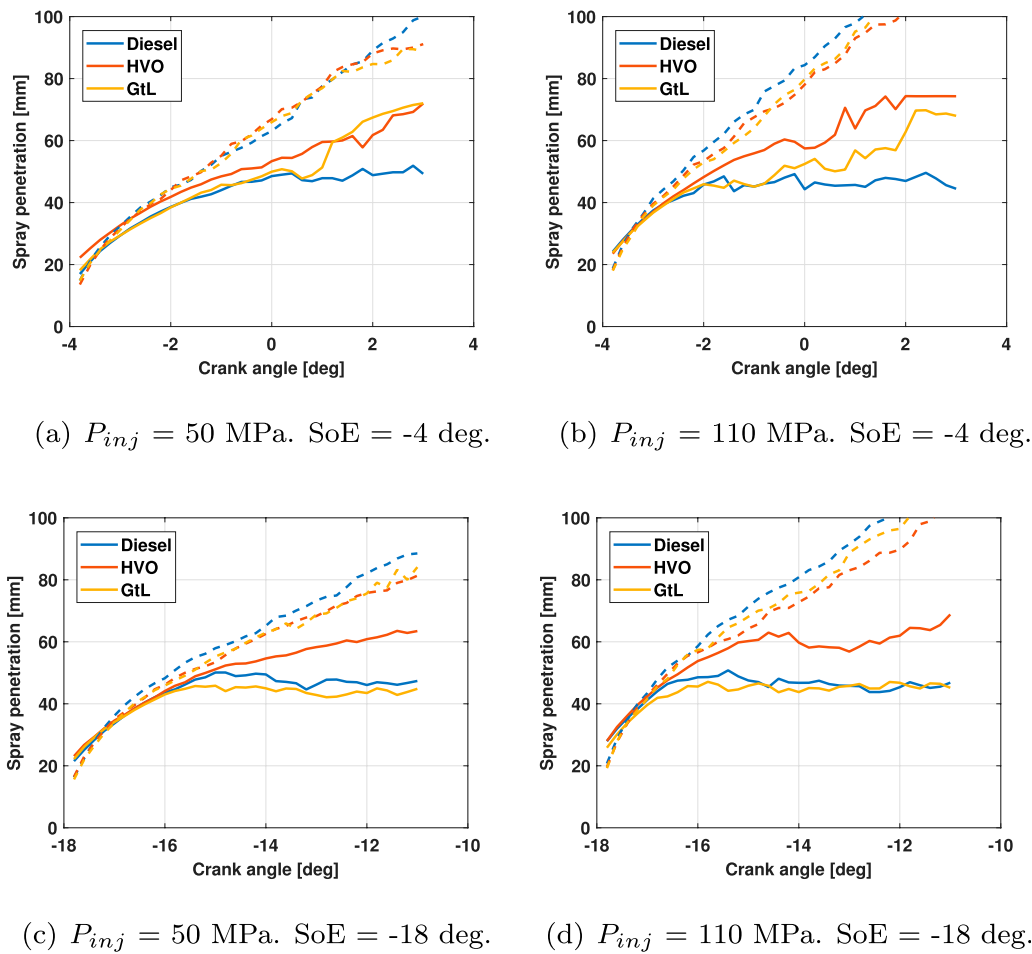


FIGURE 11 Experimental (solid line) and modelled (dashed line) spray penetration as a function of crank angle for each fuel. (a) $P_{inj} = 50$ MPa, SoE = -4 deg, (b) $P_{inj} = 70$ MPa, SoE = -4 deg, (c) $P_{inj} = 90$ MPa, SoE = -8 deg, (d) $P_{inj} = 110$ MPa SoE = -18 deg.

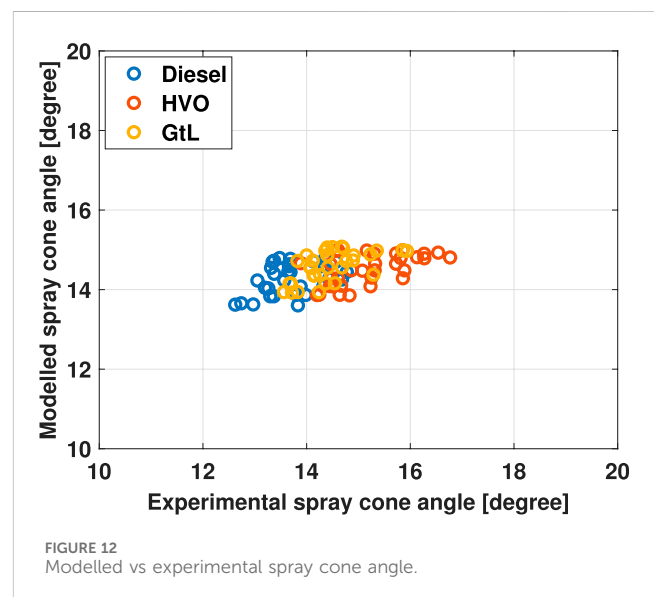
considers that the spray is non-evaporative, the combustion chamber environment is at rest, the spray momentum is constant in time and the radial velocity distribution is Gaussian. Also, the cone angle model proposed by Siebers (2009), shown in Equation 6, considers the combustion chamber environment at rest.

It can be noted that the model results are consistent with experimental measurements for a short time after SoI where the portion of the jet that has vapourised is negligible.

Figure 12 shows how the results obtained with Equation 6 are of the same order as the experimental ones. It also indicates that the dispersion of the results is small. The experimental mean spray cone angle is lower for diesel, higher for HVO fuel and intermediate for GtL fuel.

This is a very interesting result. On the one hand, the model also predicts the effect of fuel properties on the evolution of the spray cone angle, although with a narrower range (between 13.5 and 15° in modelling) while experimental results are between 12.5 and 17°. On the other hand, although the ignition delay clearly correlates with the cetane number of fuels (higher cetane number leads to shorter ignition delay), the model result helps to confirm the order in ignition delay of fuels tested.

However, at the same in-cylinder thermodynamic conditions, a slightly wider cone angle is modelled and experimentally observed



with HVO fuel. A slightly wider cone angle of the HVO fuel spray could be leading to a slightly higher air entrainment. This last fact

could be collaborating in an additional shortening of the HVO fuel ignition delay.

4 Conclusions and future works

In this study, the spray macroscopic parameters, ignition delay and the estimation spray surface of HVO, GtL and diesel fuels have been determined. This has been achieved at an experimental facility with a compression ignition engine with optical access that allows the injection and combustion processes to be visualized. Schlieren optical technique produces images able to provide quantitative information. The experimental tests were carried out at different selected injection pressures and different starts of injector energization (SoE) times. The main conclusions obtained are summarized below.

- Under the thermodynamic conditions tested the spray cone angle is not strongly influenced by the injection pressure, the start of energization (SoE), or the physical and chemical properties of the fuel.
- An increase in injection pressure produces a reduction in the stabilization time of spray penetration, generating greater spray penetration for the same energization time. Therefore, a larger spray surface area is generated, a greater air-fuel mixture, better combustion and a reduction in pollutant emissions. This conclusion is consistent for a constant spray cone angle.
- An earlier start of energization (SoE) leads to a discharge against a reduced density of the air in the combustion chamber, the in-cylinder pressure and temperature. For the fuels with low density, low surface tension and a lower fuel distillation curve, it generates a reduction in the spray penetration and the spray surface. This means a lower air-fuel mixture, larger combustion delay, poor combustion and an increase in polluting emissions. This conclusion is also consistent for a constant spray cone angle.
- Although the models used for predicting spray penetration and its cone angle correspond to non-evaporative, they provide good results, showing a good concordance at the beginning of the injection process between modelled and experimental results, independently of the fuel used.
- Estimated ignition delay (ID) is mainly influenced by the injector start of energization (SoE) time and by the cetane number of the fuel. At early starts of energization, the cetane number of the fuel has less influence on the ignition delay than at later energization starts, where the ambient pressure, temperature and density values are higher. A higher cetane number results in a reduced ignition delay (ID).
- In the range of injection pressure tested, no clear effect on ignition delay is detected probably due to: i) in the commented range, for this type of engine, the effect of cetane number of fuels is more important than the effect of the injection pressure, itself, ii) the automatic image processing procedure does not have enough sensibility to clearly detect the ignition delay variations in the analyzed range.

HVO fuel exhibits better air-fuel mixture capabilities than the other two fuels. Since it shows a larger spray surface for all injection pressures and all start of energization (SoE) times. Furthermore, later start of injector energization results in shorter ignition delay

and earlier start of combustion. The measurement of the variation of spray evolution with the conditions within the cylinder and the fuel used, allow for a better tuning of the injector start of energizing and to assess the need of swirl in the intake valve port for a better fuel-air mixing. These details are relevant in the optimization of the power to weight ratio that determines the performance of the aircraft.

The work done, and here presented, will be extended to: i) fuel blends composed by renewable sustainable kerosenes and fossil diesel fuels, ii) other different thermodynamic engine conditions coupling to the engine an altitude simulation machine, and iii) the complete spray evolution, comparing it to model predictions under different evaporative conditions.

Data availability statement

The raw data supporting the conclusions of this article will be made available by the authors, without undue reservation.

Author contributions

LC-G: Data curation, Formal Analysis, Investigation, Software, Validation, Visualization, Writing – original draft, Writing – review and editing. OA: Conceptualization, Funding acquisition, Methodology, Project administration, Resources, Supervision, Writing – original draft, Writing – review and editing. FM-F: Data curation, Formal Analysis, Software, Visualization, Writing – original draft, Writing – review and editing. JS: Data curation, Investigation, Methodology, Validation, Visualization, Writing – original draft, Writing – review and editing. FM: Data curation, Formal Analysis, Methodology, Software, Validation, Writing – original draft, Writing – review and editing. JN: Writing – original draft, Writing – review and editing, Supervision, Funding acquisition, Resources.

Funding

The author(s) declare that financial support was received for the research and/or publication of this article. Financial support provided by the Castilla-La Mancha Government to the project, EXPLORA Ref. SBPLY/23/180225/000151. Financial support provided by the Ministry of Science and Innovation to the project LOOK-AHEAD Ref. PID2020-118387RB-C32.

Acknowledgments

Authors also wish to thank the collaboration of SASOL company and REPSOL Tech Lab for the supply of GTL and HVO fuels respectively.

Conflict of interest

OA reports that financial support was provided by Castilla-La Mancha Government.

The remaining authors declare that the research was conducted in the absence of any commercial or financial

relationships that could be construed as a potential conflict of interest.

Generative AI statement

The author(s) declare that no Generative AI was used in the creation of this manuscript.

References

- Aatola, H., Larmi, M., Sarjoavaara, T., and Mikkonen, S. (2009). Hydrotreated vegetable oil (HVO) as a renewable diesel fuel: trade-off between NO_x, particulate emission, and fuel consumption of a heavy duty engine. *SAE Int. J. Engines* 1, 1251–1262. doi:10.4271/2008-01-2500
- Agarwal, A. K., Srivastava, D. K., Dhar, A., Maurya, R. K., Shukla, P. C., and Singh, A. P. (2013). Effect of fuel injection timing and pressure on combustion, emissions and performance characteristics of a single cylinder diesel engine. *Fuel* 111, 374–383. doi:10.1016/j.fuel.2013.03.016
- Algayyim, S. J. M., and Wandel, A. P. (2021). Macroscopic and microscopic characteristics of biofuel spray (biodiesel and alcohols) in CI engines: a review. *Fuel* 292, 120303. doi:10.1016/j.fuel.2021.120303
- Alkhatay, S. A., Joshi, G. D., and Henein, N. (2021). Analysis and correlation of ignition delay for hydrotreated vegetable oil and ultra low sulfur diesel and their blends in ignition quality tester. *Fuel* 289, 119816. doi:10.1016/j.fuel.2020.119816
- Amhamed, A. I., Al Assaf, A. H., Le Page, L. M., and Alrebei, O. F. (2024). Alternative sustainable aviation fuel and energy (SAFE)-A Review with selected simulation cases of study. *Energy Rep.* 11, 3317–3344. doi:10.1016/j.egy.2024.03.002
- Aradi, A. A., and Ryan, T. W. (1995). Cetane effect on diesel ignition delay times measured in a constant volume combustion apparatus. *Tech. Rep.*, 952352. doi:10.4271/952352
- Arkoudeas, P., Kalligeros, S., Zannikos, F., Anastopoulos, G., Karonis, D., Korres, D., et al. (2003). Study of using JP-8 aviation fuel and biodiesel in CI engines. *Energy Convers. Manag.* 44, 1013–1025. doi:10.1016/S0196-8904(02)00112-7
- Armas, O., García-Contreras, R., Ramos, Á., and López, A. F. (2015). Impact of animal fat biodiesel, GTL, and HVO fuels on combustion, performance, and pollutant emissions of a light-duty diesel vehicle tested under the NEDC. *J. Energy Eng.* 141, C4014009. doi:10.1061/(ASCE)EY.1943-7897.0000237
- Armas, O., Martínez-Martínez, S., Mata, C., and Pacheco, C. (2016). Alternative method for bulk modulus estimation of Diesel fuels. *Fuel* 167, 199–207. doi:10.1016/j.fuel.2015.11.067
- Bjorgen, K. O. P., Emberson, D. R., and Løvås, T. (2020). Combustion and soot characteristics of hydrotreated vegetable oil compression-ignited spray flames. *Fuel* 266, 116942. doi:10.1016/j.fuel.2019.116942
- Bohl, T., Smallbone, A., Tian, G., and Roskilly, A. P. (2018). Particulate number and NO trade-off comparisons between HVO and mineral diesel in HD applications. *Fuel* 215, 90–101. doi:10.1016/j.fuel.2017.11.023
- Bohl, T., Tian, G., Smallbone, A., and Roskilly, A. P. (2017). Macroscopic spray characteristics of next-generation bio-derived diesel fuels in comparison to mineral diesel. *Appl. Energy* 186, 562–573. doi:10.1016/j.apenergy.2016.10.082
- Chen, L., Liang, Z., Liu, H., Ding, S., and Li, Y. (2017). Sensitivity analysis of fuel types and operational parameters on the particulate matter emissions from an aviation piston engine burning heavy fuels. *Fuel* 202, 520–528. doi:10.1016/j.fuel.2017.04.052
- Chen, Z., Zhao, P., Zhang, H., Chen, H., He, H., Wu, J., et al. (2024). An optical study on the cross-spray characteristics and combustion flames of automobile engine fueled with diesel/methanol under various injection timings. *Energy* 290, 130286. doi:10.1016/j.energy.2024.130286
- Choi, K., Lee, D., Roh, H. G., and Lee, C. S. (2015). Effect of injection parameters on spray characteristics of gas-to-liquid (gtl), biodiesel, and diesel fuel for a multi-hole injector in a diesel engine. *Atomization Sprays* 25, 1107–1125. doi:10.1615/AtomizSpr.2015012055
- Corral-Gómez, L., Armas, O., Soriano, J. A., Nogueira, J.-I., and Bracho, G. (2023a). Spray momentum flux novel estimation procedure through the fuel rate of injection using hydrogenated fuels with single hole nozzle diesel injector. *ACS omega* 8, 48071–48080. doi:10.1021/acsomega.3c06917
- Corral-Gómez, L., Armas, O., Soriano, J. A., Pastor, J. V., García-Oliver, J. M., and Micó, C. (2022). An optical engine used as a physical model for studies of the combustion process applying a two-color pyrometry technique. *Energies* 15, 4717. doi:10.3390/en15134717
- Corral-Gómez, L., Castillo-García, F. J., Soriano, J. A., and Armas, O. (2023b). Macroscopic parameters of fuel sprays injected in an optical reciprocating single-cylinder engine: an approximation by means of visualization with Schlieren technique. *Sensors* 23, 6747. doi:10.3390/s23156747
- Corral-Gómez, L., Martos, F. J., Fernández-Yáñez, P., and Armas, O. (2023c). A CFD modelling approach of fuel spray under initial non-reactive conditions in an optical engine. *Energies* 16, 6537. doi:10.3390/en16186537
- Corral-Gómez, L., Rubio-Gómez, G., Martínez-Martínez, S., and Sánchez-Cruz, F. (2019). Effect of diesel-biodiesel-ethanol blends on the spray macroscopic parameters in a common-rail diesel injection system. *Fuel* 241, 876–883. doi:10.1016/j.fuel.2018.12.081
- da Costa, R. B. R., Roque, L., de Souza, T., Coronado, C., Pinto, G., Cintra, A., et al. (2022). Experimental assessment of renewable diesel fuels (HVO/Farnesane) and bioethanol on dual-fuel mode. *Energy Convers. Manag.* 258, 115554. doi:10.1016/j.enconman.2022.115554
- Desantes, J. M., Payri, R., Salvador, F. J., and Gil, A. (2006). Development and validation of a theoretical model for diesel spray penetration. *Fuel* 85, 910–917. doi:10.1016/j.fuel.2005.10.023
- Dinc, A., and Otkur, M. (2021). Emissions prediction of an aero-piston gasoline engine during surveillance flight of an unmanned aerial vehicle. *Aircr. Eng. Aerosp. Technol.* 93, 462–472. doi:10.1108/AEAT-09-2020-0196
- EASA (2019). Implementation of the latest CAEP amendments to ICAO annex 16 volumes I, II and III. Available online at: <https://www.easa.europa.eu/sites/default/files/dfu/NPA%202020-06.pdf>.
- Erkkilä, K., Nylund, N.-O., Hulkkonen, T., Tilli, A., Mikkonen, S., Saikkonen, P., et al. (2011). Emission performance of paraffinic HVO diesel fuel in heavy duty vehicles. *Tech. Rep.* doi:10.4271/2011-01-1966
- Fajri, H., Rieß, S., Mallada, R. C., Ruoff, I., and Wensing, M. (2023). Optical measurements of two cylindrical and conical heavy-duty diesel injector nozzles—A comparison of reference diesel, HVO, and RME fuels. *Energy Convers. Manag.* 285, 117018. doi:10.1016/j.enconman.2023.117018
- Gajević, S., Marković, A., Milojević, S., Ašonja, A., Ivanović, L., and Stojanović, B. (2024). Multi-objective optimization of tribological characteristics for aluminum composite using taguchi grey and topsis approaches. *Lubricants* 12, 171. doi:10.3390/lubricants12050171
- Geng, L., Bi, L., Li, Q., Chen, H., and Xie, Y. (2021). Experimental study on spray characteristics, combustion stability, and emission performance of a CRDI diesel engine operated with biodiesel–ethanol blends. *Energy Rep.* 7, 904–915. doi:10.1016/j.egy.2021.01.043
- Gómez, A., Soriano, J., and Armas, O. (2016). Evaluation of sooting tendency of different oxygenated and paraffinic fuels blended with diesel fuel. *Fuel* 184, 536–543. doi:10.1016/j.fuel.2016.07.049
- Gopinath, S., Devan, P., Sabarish, V., Babu, B. S., Sakthivel, S., and Vignesh, P. (2020). Effect of spray characteristics influences combustion in di diesel engine—a review. *Mater. Today Proc.* 33, 52–65. doi:10.1016/j.matpr.2020.03.130
- Gowdagiri, S., Cesari, X. M., Huang, M., and Oehlschlaeger, M. A. (2014). A diesel engine study of conventional and alternative diesel and jet fuels: ignition and emissions characteristics. *Fuel* 136, 253–260. doi:10.1016/j.fuel.2014.07.056
- Han, D., Zhai, J., Duan, Y., Ju, D., Lin, H., and Huang, Z. (2017). Macroscopic and microscopic spray characteristics of fatty acid esters on a common rail injection system. *Fuel* 203, 370–379. doi:10.1016/j.fuel.2017.04.098
- Hansen, A. C., Zhang, Q., and Lyne, P. W. (2005). Ethanol–diesel fuel blends—a review. *Bioresour. Technol.* 96, 277–285. doi:10.1016/j.biortech.2004.04.007
- Hiroyasu, H., Kadota, T., and Arai, M. (1980). “Supplementary comments: fuel spray characterization in diesel engines,” in *Combustion Model. Reciprocating Engines Ed.*, 369–408. doi:10.1007/978-1-4899-5298-1_12
- Hulkkonen, T., Hillamo, H., Sarjoavaara, T., and Larmi, M. (2011). Experimental study of spray characteristics between hydrotreated vegetable oil (HVO) and crude oil based EN 590 diesel fuel. *Tech. Rep. SAE Tech. Pap.* doi:10.4271/2011-24-0042
- Jing, W., Roberts, W. L., and Fang, T. (2015). Spray combustion of Jet-A and diesel fuels in a constant volume combustion chamber. *Energy Convers. Manag.* 89, 525–540. doi:10.1016/j.enconman.2014.10.010

Publisher's note

All claims expressed in this article are solely those of the authors and do not necessarily represent those of their affiliated organizations, or those of the publisher, the editors and the reviewers. Any product that may be evaluated in this article, or claim that may be made by its manufacturer, is not guaranteed or endorsed by the publisher.

- Kook, S., and Pickett, L. M. (2012). Liquid length and vapor penetration of conventional, Fischer–Tropsch, coal-derived, and surrogate fuel sprays at high-temperature and high-pressure ambient conditions. *Fuel* 93, 539–548. doi:10.1016/j.fuel.2011.10.004
- Ma, Y., Huang, S., Huang, R., Zhang, Y., and Xu, S. (2016). Spray and evaporation characteristics of n-pentanol–diesel blends in a constant volume chamber. *Energy Convers. Manag.* 130, 240–251. doi:10.1016/j.enconman.2016.10.063
- Mancaruso, E., Sequino, L., and Vaglieco, B. M. (2011). First and second generation biodiesels spray characterization in a diesel engine. *Fuel* 90, 2870–2883. doi:10.1016/j.fuel.2011.04.028
- Marinković, D., Dezső, G., and Milojević, S. (2024). Application of machine learning during maintenance and exploitation of electric vehicles. *Adv. Eng. Lett.* 3, 132–140. doi:10.46793/adeletters.2024.3.3.5
- Martos, F. J., Soriano, J. A., Braic, A., Fernández-Yáñez, P., and Armas, O. (2023). A CFD modelling approach for the operation analysis of an exhaust backpressure valve used in a euro 6 diesel engine. *Energies* 16, 4112. doi:10.3390/en16104112
- Martos, F. J., Soriano, J. A., Mata, C., Armas, O., and Soto, F. (2022). Impact of alternative and fossil diesel fuels on internal flow of injection nozzle. *Int. J. Engine Res.* 23, 940–957. doi:10.1177/1468087421996525
- Mihyar, T., Şen, E., and Soyhan, H. S. (2023). Impact of the jazari technology piston motion profile on the indicated thermal efficiency of a 4-cylinder diesel engine. *Fuel* 351, 128904. doi:10.1016/j.fuel.2023.128904
- Milojević, S., Glišović, J., Savić, S., Bošković, G., Bukvić, M., and Stojanović, B. (2024). Particulate matter emission and air pollution reduction by applying variable systems in tribologically optimized diesel engines for vehicles in road traffic. *Atmosphere* 15, 184. doi:10.3390/atmos15020184
- Miron, L., Chiriac, R., Brabec, M., and Bădescu, V. (2021). Ignition delay and its influence on the performance of a diesel engine operating with different diesel–biodiesel fuels. *Energy Rep.* 7, 5483–5494. doi:10.1016/j.egy.2021.08.123
- Moser, B. R. (2009). Biodiesel production, properties, and feedstocks. *Vitro Cell. and Dev. Biology-Plant* 45, 229–266. doi:10.1007/s11627-009-9204-z
- Naber, J. D., and Siebers, D. L. (1996). Effects of gas density and vaporization on penetration and dispersion of diesel sprays. *SAE Trans.*, 960034–111doi. doi:10.4271/960034
- Neves, R. C., Klein, B. C., da Silva, R. J., Rezende, M. C. A. F., Funke, A., Olivarez-Gómez, E., et al. (2020). A vision on biomass-to-liquids (BTL) thermochemical routes in integrated sugarcane biorefineries for biojet fuel production. *Renew. Sustain. Energy Rev.* 119, 109607. doi:10.1016/j.rser.2019.109607
- Ning, L., Duan, Q., Wei, Y., Zhang, X., Yang, B., and Zeng, K. (2020). Experimental investigation on combustion and emissions of a two-stroke DISI engine fueled with aviation kerosene at various compression ratios. *Fuel* 259, 116224. doi:10.1016/j.fuel.2019.116224
- Ning, L., Duan, Q., Wei, Y., Zhang, X., Yu, K., Yang, B., et al. (2019). Effects of injection timing and compression ratio on the combustion performance and emissions of a two-stroke DISI engine fuelled with aviation kerosene. *Appl. Therm. Eng.* 161, 114124. doi:10.1016/j.applthermaleng.2019.114124
- Payri, R., Bracho, G., Soriano, J. A., Fernández-Yáñez, P., and Armas, O. (2020). Nozzle rate of injection estimation from hole to hole momentum flux data with different fossil and renewable fuels. *Fuel* 279, 118404. doi:10.1016/j.fuel.2020.118404
- Ramos, Á., García-Contreras, R., and Armas, O. (2016). Performance, combustion timing and emissions from a light duty vehicle at different altitudes fueled with animal fat biodiesel, GTL and diesel fuels. *Appl. Energy* 182, 507–517. doi:10.1016/j.apenergy.2016.08.159
- Rubio-Gómez, G., Martínez-Martínez, S., Rúa-Mojica, L. F., Gómez-Gordo, P., and De la Garza, O. A. (2018). Automatic macroscopic characterization of diesel sprays by means of a new image processing algorithm. *Meas. Sci. Technol.* 29, 055406. doi:10.1088/1361-6501/aab121
- Schaberg, P., Botha, J., Schnell, M., Hermann, H.-O., Pelz, N., and Maly, R. (2005). Emissions performance of GTL diesel fuel and blends with optimized engine calibrations. *SAE Trans.*, 1074–1087doi. doi:10.4271/2005-01-2187
- Schihl, P., Gingrich, E., and Decker, L. (2015). The combustion and ignition characteristics of varying blend ratios of JP-8 and a coal to liquid Fischer–Tropsch jet fuel in a military relevant single cylinder diesel engine. *SAE Int. J. Fuels Lubr.* 8, 501–514. doi:10.4271/2015-01-9073
- Settles, G. S. (2001). *Schlieren and shadowgraph techniques: visualizing phenomena in transparent media*. Springer Science and Business Media.
- Siebers, D. L. (2009). “Recent developments on diesel fuel jets under quiescent conditions,” in *Flow and combustion in reciprocating engines*, 257–308doi. doi:10.1007/978-3-540-68901-0_5
- Soid, S., and Zainal, Z. A. (2011). Spray and combustion characterization for internal combustion engines using optical measuring techniques—A review. *Energy* 36, 724–741. doi:10.1016/j.energy.2010.11.022
- Soriano, J., García-Contreras, R., Gómez, A., and Mata, C. (2019). Comparative study of the effect of a new renewable paraffinic fuel on the combustion process of a light-duty diesel engine. *Energy* 189, 116337. doi:10.1016/j.energy.2019.116337
- Sugiyama, K., Goto, I., Kitano, K., Mogi, K., and Honkanen, M. (2012). Effects of hydrotreated vegetable oil (HVO) as renewable diesel fuel on combustion and exhaust emissions in diesel engine. *SAE Int. J. Fuels Lubr.* 5, 205–217. doi:10.4271/2011-01-1954
- ul Haq, M., Jafry, A. T., Ahmad, S., Cheema, T. A., Kamran, M., Ajab, H., et al. (2023). Macroscopic spray behavior in pressurized chamber alongside thermal performance of quaternary castor biodiesel with butanol and 1-butoxybutane. *Energy* 282, 128912. doi:10.1016/j.energy.2023.128912
- Wu, T., Huang, Z., Zhang, W.-g., Fang, J.-h., and Yin, Q. (2007). Physical and chemical properties of GTL-diesel fuel blends and their effects on performance and emissions of a multicylinder DI compression ignition engine. *Energy and Fuels* 21, 1908–1914. doi:10.1021/ef0606512

Nomenclature

A	Area
c_1	constant
c_2	constant
C_d	Discharge coefficient
CI	Compression ignition
C_v	Velocity coefficient
D	Diameter
K	constant
\dot{m}	Mass flow rate
\dot{M}	Momentum flux
P	Pressure
S	Spray penetration
SI	Spark ignition

T	Temperature
t	Time
u	Velocity
θ	Spray cone angle
ρ	Density

Subscripts

a	Ambient
B	Bernoulli
f	Fuel
inj	Injection
h	Hole